A Lumped-Parameter Model for Nonlinear Waves in Graphene*

Hamad Hazim[1], Dongming Wei[2], Mohamed Elgindi[1], Yeran Soukiassian[1]

[1] Texas A & M University-Qatar, Doha, Qatar
[2] Nazarbayev University, Astana, Kazakhstan

Abstract

A lumped-parameter nonlinear spring-mass model which takes into account the third-order elastic stiffness constant is considered for modeling the free and forced axial vibrations of a graphene sheet with one fixed end and one free end with a mass attached. It 's demonstrated through this simple model that, in free vibration, within certain initial energy level and depending upon its length and the nonlinear elastic constants, there exist bounded periodic solutions which are non-sinusoidal, and that for each fixed energy level, there is a bifurcation point depending upon material constants, beyond which the periodic solutions disappear. The amplitude, frequency, and the corresponding wave solutions for both free and forced harmonic vibrations are calculated analytically and numerically. Energy sweep is also performed for resonance applications.

Keywords: Graphene, Resonance, Nonlinear Vibration, Phase Diagram, Frequency Sweep
AMS Subject Classification: 35B10; secondary 70K30, 73K05

1 Introduction

The graphene-based resonator and its application to mass sensing based on nonlinear waves have been poorly studied numerically [1]. Some researchers use discrete atomic or Monte Carlo approach for numerical simulation and some use local or nonlocal continuum mechanics approaches, however, their models are based on linear material constitutive equation for graphene ([1],[2],[3],[4]). It is, however, well-known that graphene behaves

*World Journal of Engineering and Technology, 2015, 3, 57-69 Published Online May 2015 in SciRes. http://www.scirp.org/journal/wjet http://dx.doi.org/10.4236/wjet.2015.32006

nonlinearly even for small strains and there is no obvious yield point or a linear portion on its stress-strain curve. In fact, it is proved experimentally in [5] and theoretically in [6] that the mechanical behavior of a single layer of graphene sheet can be accurately modeled by a continuum nonlinear constitutive equation (also see, [7],[8],[9],[10]). This constitutive equation in one dimensional form is:

$$\sigma = E\epsilon + D|\epsilon|\epsilon \tag{1}$$

where ϵ is the axial strain, σ the axial stress, E the Young's modulus, $D = -\frac{E^2}{4\sigma_{max}}$ the third-order elastic stiffness constant, and σ_{max} the ultimate yield stress of the graphene. Equation (1) is valid only for $|\sigma| \leq \sigma_{max}$. It appears that recent studies in literature have not incorporated the constant D into their models for the vibration analysis of graphene layers. The main objective of this work is to model and understand how graphene behaves in free and forced axial vibrations and to calculate the nonlinear resonance frequencies based on equation (1). To initiate this study, a simplified nonlinear spring model is derived based on the lumped parameter method. We show that the third-order elastic stiffness D plays an important role in modeling the patterns of graphene in axial vibration. Within a range of the initial energy, we show that there exist periodic solutions similar to the ones obtained using the corresponding linear models and that the free oscillations are nearly sinusoidal. However, as the initial energy approaches a threshold level, the limiting free oscillations deviate drastically from the sinusoidal oscillations predicted by linear models. Our initial results provide some quantitative regimes in which a graphene resonator can operate near harmonic and non-harmonic motions. The initial results of this project provide some insight information and data on the patterns of axial vibration of a graphene monolayer which can be useful for design of graphene-based resonators. By extending this simple nonlinear spring-mass model to more realistic models, it is possible to provide new design guide to help make more efficient resonators and wave guides, shorten the design cycle and provide more accurate assessment of the mechanical behavior of these devices. For example, in [4], a mechanically vibrating graphene-diaphragm based audio resonator was studied experimentally, and the linear elastic theory in [11] for circular diaphragm was used to predict the maximum displacement and maximum strain in the graphene. It is found that the predicted value of the maximum strain is well below the breaking strain of graphene obtained experimentally. Our study clearly indicates that the linear theory is inadequate since it does not take

into account the effect of the nonlinear term in (1). Therefore, by expanding our study for the diaphragm can help design a better graphene audio speaker in this case. In section 2, we derive the nonlinear spring lumped parameter model from the nonlinear wave equation of a graphene sheet under axial vibration; in section 3, we study the existence of periodic solutions by using phase plane analysis and perturbation techniques; in section 4, we compute the approximate analytical solutions of free vibrations using the two-scales splitting method and obtain the associated natural frequencies and amplitudes and compare to numerical results; in section 5, we compute numerical solutions of forced vibrations and obtain frequency sweeps.

2 The nonlinear lumped parameter model

A graphene sheet with uniform cross-section in axial vibration with one fixed-free end can be modeled by substituting (1) into the standard balance of momentum equation $\rho\ddot{u} = \sigma' + f$ to obtain the following nonlinear wave equation subject to initial and boundary conditions :

$$\begin{cases} \rho\ddot{u} = Eu'' + D(|u'|u')' + f(x,t), x \in (0,L), t > 0 \\ u(x,0) = u_0, \dot{u}(x,0) = 0, x \in (0,L) \\ u(0,t) = 0, \sigma(L,t) = f_0(t) \end{cases} \tag{2}$$

Here we use $\ddot{u}$ for second order time derivative of u and u' for spatial derivative of u. The corresponding steady state problem with a concentrated load of magnitude f_0 at the tip $x = L$ and without distributed load along the length of the rod is

$$\begin{cases} Eu'' + D(|u'|u')' = 0, x \in (0,L) \\ u(0) = 0, \sigma(L) = f_0 \end{cases} \tag{3}$$

Assuming that $|f_0| \leq \sigma_{max}$, the exact solution of (3) can be found by integrating it and applying the boundary conditions. We get:

$$u(x) = \begin{cases} \frac{2\sigma_{max}}{E}(1 - \sqrt{1 - \frac{f_0}{\sigma_{max}}})x, f_0 > 0 \\ \frac{2\sigma_{max}}{E}(-1 + \sqrt{1 + \frac{f_0}{\sigma_{max}}})x, f_0 \leq 0 \end{cases} \tag{4}$$

Equation (4), then, provides the relationship between the applied force f_0 at the tip and the tip-displacement $u(L)$ as:

$$f_0 = EX + D|X|X, X = \frac{u(L)}{L} \tag{5}$$

Our lumped parameter model is based on imposing a boundary condition at $x = L$ with an additional inertial force $-m\ddot{u}(L,t)$ and using the following calculations: For fixed time t, integrating the equation $Eu'' + D(|u'|u')' = 0$ over $[0, L]$ with boundary conditions $u(0,t) = 0, \sigma(L,t) = f_0(t) - m\ddot{u}(L,t)$ gives:

$$u(L,t)) = \begin{cases} \frac{2\sigma_{max}}{E}(1 - \sqrt{1 - \frac{f_0 - m\ddot{u}(L,t)}{\sigma_{max}}})L, f_0 - m\ddot{u}(L,t) > 0 \\ \frac{2\sigma_{max}}{E}(-1 + \sqrt{1 + \frac{f_0 - m\ddot{u}(L,t)}{\sigma_{max}}})L, f_0 - m\ddot{u}(L,t) \leq 0 \end{cases} \tag{6}$$

Equation (6) gives the following nonlinear spring-mass equation in which $u(L,t)$ is denoted by x:

$$m\ddot{x} + \frac{E}{L}x + \frac{D}{L^2}|x|x = f_0(t) \tag{7}$$

where m is the lumped-mass at the tip of the sheet, E is the first order stiffness and D is the third-order stiffness constant in (1). Using the change of variable $t = \sqrt{\frac{E}{mL}}\tau$ we obtain the equivalent non-dimensional equation

$$\ddot{x} + x - \alpha x|x| = \hat{f}(t) \tag{8}$$

where $\alpha = \frac{E}{4L\sigma_{max}}$ is a positive parameter and $\hat{f}(t) = \frac{Lf_0}{E}$.

3 Existence of periodic solutions of free vibration

We will show that for given initial conditions $x(0)$ and $\dot{x}(0)$, equation (8) has periodic solutions for certain range of α . To determine the ranges of α for which existence of periodic solutions occur, we examine the phase diagrams associated with equation (8) defined by:

$$\frac{y^2}{2} = \frac{-x^2}{2} + \frac{1}{3}\alpha x^2|x| + C, \tag{9}$$

where $y = \dot{x}$. We make the following observations:
(1) The y-intercepts associated with (9) are $y = \pm\sqrt{2C}$,
(2) C represents the energy at initial position $x = 0$,
(3) when $\alpha = 0$, the phase diagrams are the circles $y^2 + x^2 = 2C$ with center

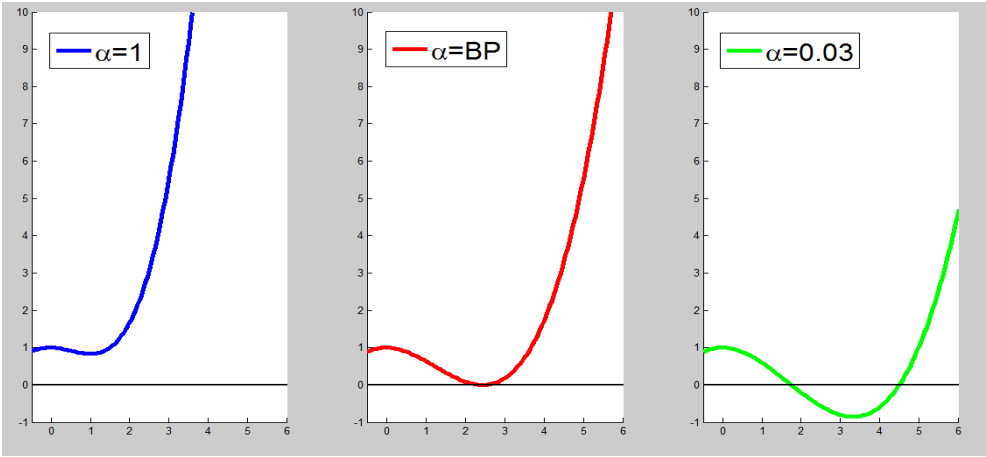

Figure 1: $y = \frac{-x^2}{2} + \frac{1}{3}\alpha x^2|x| + 1$, for (a) $\alpha = 1$, (b) $\alpha = \frac{1}{\sqrt{6}}$ and (c) $\alpha = 0.3$

$(0,0)$ and radius $\sqrt{2C}$.

We prove that for any $C > 0$, there exists α_0 such that for $\alpha \leq \alpha_0$ equation (8) has a periodic solution and for $\alpha > \alpha_0$ there exists no periodic solutions of (8). Since periodic solutions of (8) correspond to closed curves of the phase diagram, we need to examine the x-intercepts of (9) and their dependence on the equation parameters. The x-intercepts of (9) are the zeros of:

$$f(x) = \frac{-x^2}{2} + \frac{1}{3}\alpha x^2|x| + C,$$

which is an even function. Therefore it is enough to consider $f(x)$, for $x > 0$. Some properties of $f(x)$ are: $f(0) = C > 0$;$f'(x) > 0$ for $x > \frac{1}{\alpha}$ and $f'(x) < 0$ for $x < \frac{1}{\alpha}$, since $f'(x) = x(|x|\alpha - 1)$; and $f(\frac{1}{\alpha}) = C - \frac{1}{6\alpha^2}$. Based on these properties we can distinguish the following three cases (corresponding to Figures 1(a)-1(c) when C=1):
Case (a): $\alpha > \frac{1}{\sqrt{6C}} \Longrightarrow f(\frac{1}{\alpha}) > 0 \Longrightarrow$ No periodic solution .
Case (b): $\alpha = \frac{1}{\sqrt{6C}} \Longrightarrow f(\frac{1}{\alpha}) = 0 \Longrightarrow$ Only one x-intercept and there is a periodic solution.
Case (c): $\alpha < \frac{1}{\sqrt{6C}} \Longrightarrow f(\frac{1}{\alpha}) < 0 \Longrightarrow$ Two x-intercepts and there is a periodic solution.

We conclude that the bifurcation point for a given $C > 0$, is $\alpha_0^\star = \frac{1}{\sqrt{6C}}$, see Figure 2.

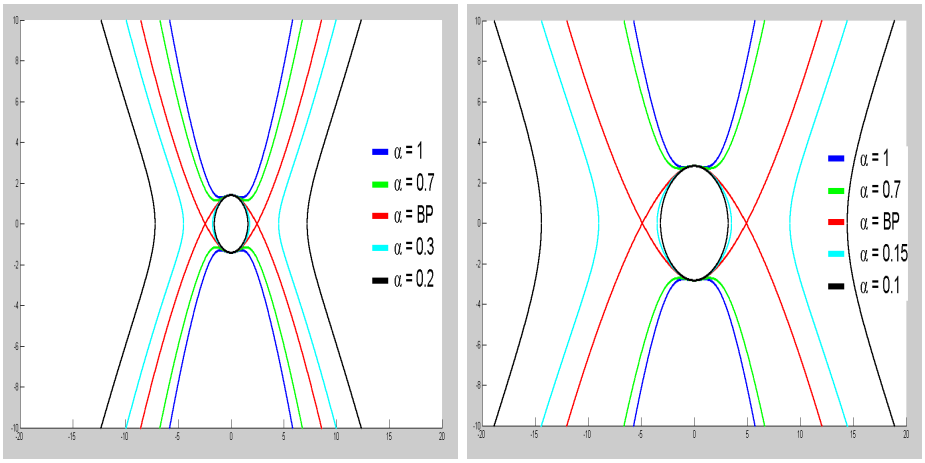

Figure 2: Left: Phase diagrams for $C = 1$ and different values of α; Right: Phase diagrams for $C = 4$ and different values of α

For a given value of $C > 0$, and for each α when periodic solution exists, we determine the smallest x-intercept of $f(x)$, call it x^* and determine the period $T(C, \alpha)$ numerically using the integral

$$T(C, \alpha) = 4 \int_0^{x^*} \frac{-dx}{\sqrt{-x^2 + \frac{2}{3}\alpha x^2 |x| + 2C}}$$

Our numerical results with $C = 1$ for the periods and frequencies corresponding to different values of α (for which periodic solutions exist) are shown in Figure 3. It is demonstrated in Figure 2 that at a lower energy level (C=1) the free vibration is approximately sinusoidal, however at a higher level of energy (C=4) the free vibration deviate drastically from the sinusoidal pattern which has not been captured by previous models that do not include the third order elastic constant D. When periodic solutions exist, according to our model, Figure 3 shows that at each fixed energy level, the frequency and period of the first mode for a given graphene sheet depend nonlinearly on the parameter α which depend on the material elastic constants as well as the length of the sheet.

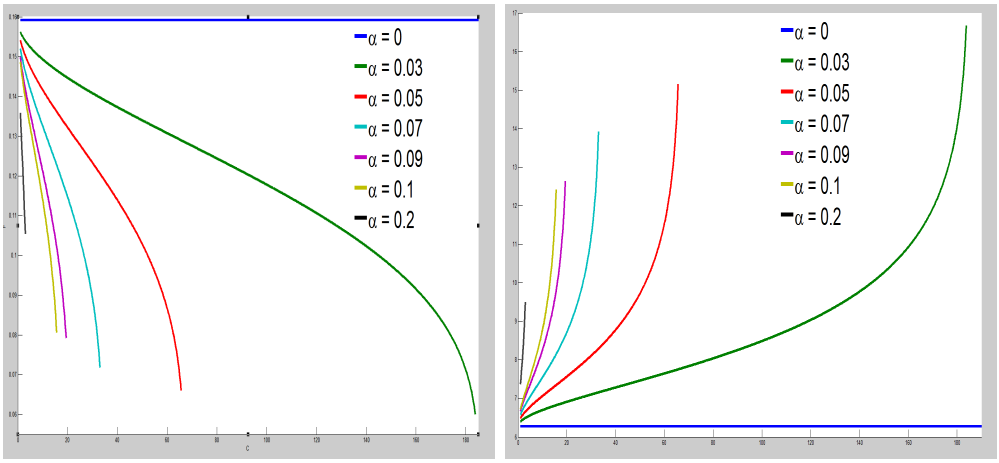

Figure 3: Left: Frequency Diagram;Right: Period Diagram

4 Double Scales Analytical Approximations of Free Vibration

Multiple scales method is often used to solve nonlinear equations with small parameters in nonlinear vibrations. Double scales are used herein to find an approximate solution of the first order for equation (8). The solution is then compared to results obtained by numerical integration using Matlab. In the following, we will use t instead of τ in equation (8). The new time scales are $T_0 = t$, $T_1 = \alpha t$ where T_0 represents the fast time and T_1 represents the slow time. The derivative with respect to t will be written as a function of the derivative with respect to T_0, T_1:

$$\begin{aligned} \frac{\partial}{\partial t} &= \frac{\partial}{\partial T_0} + \alpha \frac{\partial}{\partial T_1}, \\ \frac{\partial^2}{\partial^2 t} &= \frac{\partial^2}{\partial^2 T_0} + 2\alpha \frac{\partial^2}{\partial T_0 \partial T_1} + \alpha^2 \frac{\partial^2}{\partial^2 T_1}. \end{aligned} \tag{10}$$

Instead of determining the solution as a function of t, we determine it as a function of T_0 and T_1. To this end, we change the independent variable in equation (8) from t to T_0 and T_1. A solution of the equation is sought to have the following form:

$$x = x_0(T_0, T_1) + \alpha x_1(T_0, T_1) + O(\alpha) \tag{11}$$

Substituting (11) in (8) and identifying the term of the same power of α we obtain the following system of initial value problems:

$$\frac{\partial^2 x_0}{\partial^2 T_0} + x_0 = 0, \quad x_0(0) = a_0, \dot{x_0}(0) = 0, \tag{12}$$

$$\frac{\partial^2 x_1}{\partial^2 T_0} + x_1 = -2\frac{\partial^2 x_0}{\partial T_0 \partial T_1} + |x_0|x_0, \quad x_1(0) = 0, \dot{x_1}(0) = 0. \tag{13}$$

We will show that the solutions of equations (12) and (13) are given by:

$$\begin{aligned} x_0 =& a(T_1)\cos(T_0 + \varphi(T_1)), \\ x_1 =& \alpha_1 \cos(T_0 + \gamma_1) + \frac{2a_0|a_0|}{6\pi}\cos(3T_0 + 3\varphi(T_1)) \\ & - \frac{4a_0|a_0|}{\pi}\frac{1}{1-(2k+1)^2}\sum_{k=2}^{+\infty}\frac{(-1)^k}{4k^2-1}\cos\left((2k+1)(T_0+\varphi(T_1))\right) \\ & - \frac{4a_0|a_0|}{\pi}\frac{1}{1-(2k-1)^2}\sum_{k=2}^{+\infty}\frac{(-1)^k}{4k^2-1}\cos\left((2k-1)(T_0+\varphi(T_1))\right), \end{aligned} \tag{14}$$

where $a(T_1) = a_0$ and $\varphi(T_1) = \frac{-4|a_0|}{3\pi}T_1$. The solution of equation (8) will then be given by:

$$\begin{aligned} x(t) =& a_0\cos(1-\alpha\frac{4|a_0|}{3\pi})t + \alpha\alpha_1\cos(t+\gamma_1) + \alpha\frac{2a_0|a_0|}{6\pi}\cos 3(1-\alpha\frac{4|a_0|}{3\pi}t) \\ & - \alpha\frac{4a_0|a_0|}{\pi}\frac{1}{1-(2k+1)^2}\sum_{k=2}^{+\infty}\frac{(-1)^k}{4k^2-1}\cos\left((2k+1)(1-\alpha\frac{4|a_0|}{3\pi})t\right) \\ & - \alpha\frac{4a_0|a_0|}{\pi}\frac{1}{1-(2k-1)^2}\sum_{k=2}^{+\infty}\frac{(-1)^k}{4k^2-1}\cos\left((2k-1)(1-\alpha\frac{4|a_0|}{3\pi})t\right) \end{aligned} \tag{15}$$

Proof The solution of equation (12) has the following form:

$$x_0 = a(T_1)\cos(T_0 + \varphi(T_1)) \tag{16}$$

Substituting x_0 in (13) and writing $|x_0|$ as the Fourier series:

$$|\cos(T_0+\varphi)| = \frac{2}{\pi} - \frac{4}{\pi}\sum_{k=1}^{+\infty}\frac{(-1)^k}{4k^2-1}\cos(2k(T_0+\varphi)),$$

the following equation is obtained

$$\frac{\partial^2 x_1}{\partial^2 T_0} + x_1 = 2\frac{\partial a}{\partial T_1}\sin(T_0 + \varphi(T_1)) + 2a\frac{\partial \varphi(T_1)}{\partial T_1}\cos(T_0 + \varphi(T_1)) + \frac{2|a|}{\pi}\cos(T_0 + \varphi(T_1)) - \frac{4|a|}{\pi}\sum_{k=1}^{\infty}\frac{(-1)^k}{4k^2-1}\cos(2k(T_0 + \varphi(T_1))\cos(T_0 + \varphi(T_1)). \tag{17}$$

To avoid unbounded solutions, we set the secular terms of the x_1-equation (17), containing $\cos(T_0 + \varphi(T_1))$ and $\sin(T_0 + \varphi(T_1))$ to zero. This gives the system:

$$\begin{cases} \dfrac{\partial a}{\partial T_1} = 0, \quad a(0) = a_0 \\ 2a\dfrac{\partial \varphi(T_1)}{\partial T_1} + \dfrac{4a|a|}{3\pi} = 0, \quad \varphi(0) = 0 \end{cases}$$

whose solution gives $a(T_1) = a_0$ and $\varphi(T_1) = -\frac{4a|a_0|}{3\pi}T_1$. The solution for x_0 is then obtained by returning to the original time using $T_1 = \alpha t$.
To find x_1, we need to solve the linear differential equation:

$$\frac{\partial^2 x_1}{\partial^2 T_0} + x_1 = -\frac{4a_0|a_0|}{\pi}\sum_{k=2}^{+\infty}\frac{(-1)^k}{4k^2-1}\cos(2k(T_0 + \varphi(T_1))\cos(T_0 + \varphi(T_1)). - \frac{2a_0|a_0|}{3\pi}\cos(3(T_0 + \varphi(T_1))), \quad x_1(0) = 0, \dot{x_1}(0) = 0.$$

and obtain (14), where α_1 and γ_1 are determined easily from the initial conditions. Using t instead of T_0 and αt instead of T_1 and replacing a and φ by its values, the expression in equation (15) is verified.

Remark The solution for x_1 shows an odd multiple of the $(T_0 + \varphi(T_1))$, this can be seen clearly in the expression for x_1. These frequencies are the harmonics of the main mode or frequency. It is a typical feature of nonlinear differential equations that the harmonics are related directly to the nonlinear terms. Our expressions are verified numerically by calculating the solution in the frequency domain using the fourier transform and comparing with the analytical results.

The results in time and frequency domains are shown below in Figures 4 and 5.

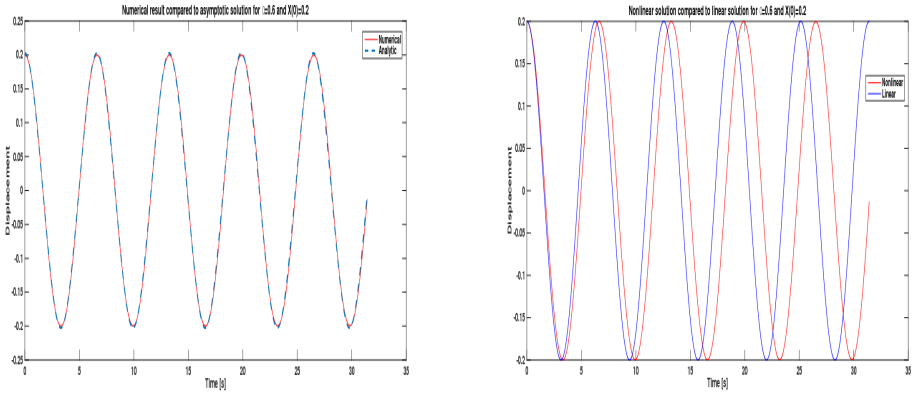

Figure 4: Left: Numerical solution compared to approximate analytical solution for $\alpha = 0.6$ and $x(0) = 0.2$. Right: Linear solution compared to nonlinear numerical solution $\alpha = 0.6$ and $x(0) = 0.2$.

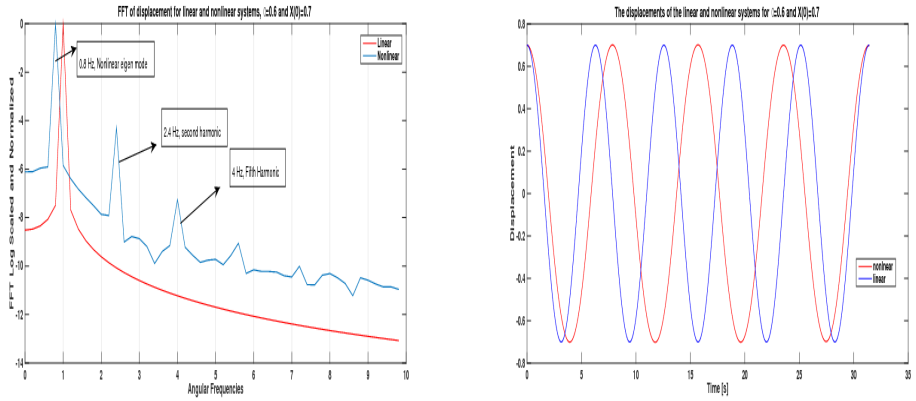

Figure 5: Left: FFT of the nonlinear solution compared to the linear solution for $\alpha = 0.6$ and $x(0) = 0.7$. Right: Linear solution compared to nonlinear numerical solution for $\alpha = 0.6$ and $x(0) = 0.7$.

5 Nonlinear vibration under harmonic excitation

In this section we characterize the nonlinear spring equation (10) by a harmonic excitation and study the system's nonlinear responses. The equation of motion is given by:

$$\ddot{x} + x + 2\xi\dot{x} - \alpha x|x| = f\cos(\omega t), \quad x(0) = 0, \dot{x}(0) = 0, \tag{18}$$

where $\omega = 1 + \omega_0$, ω_0 is a small real number called detuning parameter, and ξ is the damping coefficient.

Remark : In [4], the frequency range of an electrostatic graphene loudspeaker is studied experimentally, in which air damping and an effective linear spring constant are used to model vibration of a graphene circular membrane. It appears that in this study, the effect of the nonlinear term $\alpha x|x|$ which depends on second order stiffness constant has not been considered.

The frequency ω of the excitation is near the resonance of the corresponding linear frequency of the equation $\ddot{x} + x = 0$. We present the numerical solutions in time and frequency domains and demonstrate the use of the frequency sweep method in detecting the nonlinear resonance of the system. We solve equation (18) using Matlab solver to obtain numerical results in the time domain. FFT algorithm is then applied to the time signal to find the frequencies of the solutions. The expected frequency corresponds to the excitation ω, the nonlinear resonance and some harmonics. The double scales method can be used to find analytical approximate solution of equation (18) similar to the autonomous system case of section 4. We present our numerical results in Figure 6.

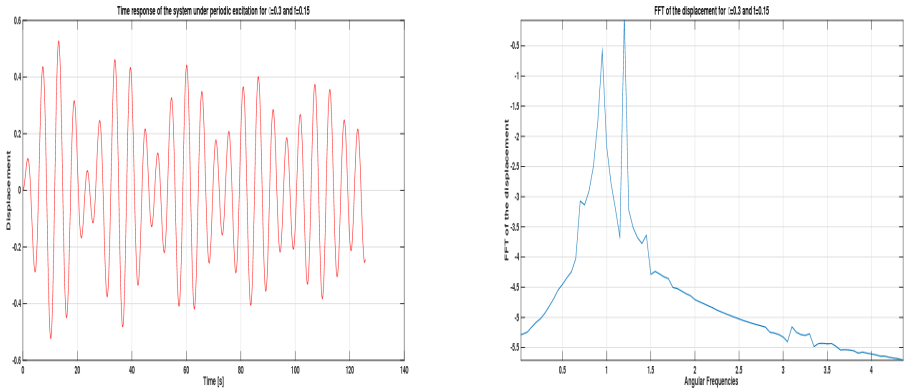

Left: Time solution for $\alpha = 0.15$ and $x(0) = 0$ and $f = 0.15$ and $\omega = 1.2$. Right: FFT of the time signal

We use the frequency sweep method to detect nonlinear resonance of the nonlinear system by direct integration. The method begins by defining a grid of frequencies around the linear resonance and intergrate the system at each point of the grid. The maximum displacement of the solution is then plotted against the frequency mesh. The curve shows a peak corresponding to the nonlinear resonance of the system. Our numerical results present the dependence of the nonlinear frequency on the magnitude of excitation and on the parameter α. Figures 7 and 8 below show the numerical results for some values of the system parameters.

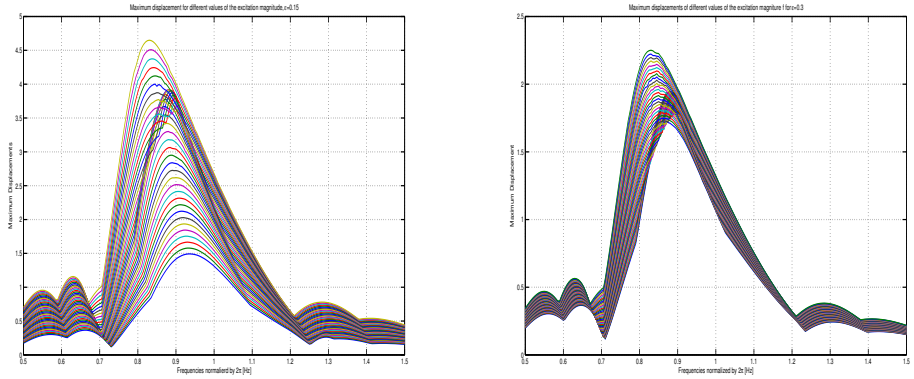

Figure 6: Left: frequency sweep for $\alpha = 0.15$ and for different values of f. Right: frequency sweep for $\alpha = 0.3$ and for different values of f

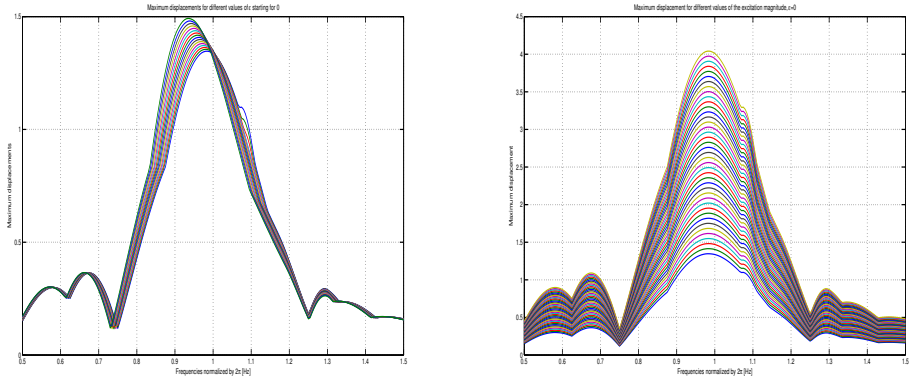

Figure 7: Left: frequency sweep for different values of α at the same magnitude f. Right: frequency sweep for the linear system for different values of f

6 Conclusions

A simplistic nonlinear spring model is derived from the axial wave equation of a graphene sheet based on the quadratic constitutive stress-strain equation. Using phase plane analysis, existence of periodic wave solutions and bifurcation points depending on the parameter $\alpha = \frac{E}{4L\sigma_{max}}$ are verified for free vibrations. Perturbation method of time scales depending on α is used to study axial vibrations subject to harmonic excitation. The results are compared with the corresponding linear spring model which does not include the third order elastic constant $D = -\frac{E^2}{4\sigma_{max}}$. It is demonstrated through our analysis and numerical solutions that the bifurcation parameter α critically affects the solutions quantitatively and numerically, therefore we conclude that the third order elastic constant D in the continuum mechanics based modeling of graphene should be included in further study of the dynamic behavior if higher accuracy of solutions are desired. In future studies we plan to examine the axial vibrations corresponding to the full model (2) numerically using finite differences, finite element and numerical bifurcation techniques. In addition, we plan to examine the vertical vibrations using nonlinear beam and plate equations.

7 Acknowledgment

The paper's first co-author acknowledges the funding provided by the NPRP grant 08-777-1-141 from the Qatar National Research Fund (a member of Qatar Foundation) to Prof. Prabir Daripa of Texas A& M University at College Station, TX 77842, USA while working on this project.

References

[1] M. D. Dai et al., Nonlinear Vibration Vehavior of Graphene Resonators and Their Applications in Sensitive Mass Detection, *Nanoscale Research Letters* , 7 (2012) pp.499-509.

[2] J. Atalaya, A. Isacsson, and J.M. Kinaret, Continuum Elastic Modeling of Graphene Resonators. *Nano letters*, 8(12) (2008) pp.4196-4200.

[3] M. E. Suggs, Graphene Resonators Analysis and Film Transfer, *Sandia Report*, SAND2012-4433, Unlimited Release, 2012.

[4] Q. Zhou and A. Zettl, Electrostatic Graphene Loudspeaker, Applied Physics Letters, 102 (2013) pp.223109-5.

[5] C. Lee et al., Measurement of the Elastic Properties and Intrinsic Strength of Monolayer Graphene, *Science*, Vol. 321, no. 5887, (2008) pp. 385-388.

[6] Q. Lu and R. Huang, Nonlinear Mechanics of Single-Atomic-Layer Graphene Sheets, *International Journal of Applied Mechanics*, Vol. 1, No. 3 (2009) pp.443-467.

[7] E. Cadelano, Graphene Under Strain-A Combined Continuum-Atomistic Approach, Ph.D. Thesis, 2010.

[8] E. Cadelano et al., Nonlinear Elasticity of Monolayer Graphene, *PRL* 102, 235502 (2009) pp. 1-4.

[9] K.C. Schwab and M.L. Roukes, Putting Mechanics into Quantum Mechanics, *Physics Today*, 58(7) (2005) pp. 36-42.

[10] S. Kuma rand D. Parks, Invariant-Theoretic Approach to Nonlinear Hyperelastic Constitutive Modeling of Graphene, arXiv:1407.1893v1, 2014.

[11] G.M. Rebeiz, RF MEMS Theory, Design, and Technology, Wiley-Interscience, 2002